Pergamon

NanoStructured Materials, Vol. 5, No. 4, pp. 383-392, 1995

0965-9773/95 $9.50 + .00

0965-9773(95)00260-X

FORMATION OF SUPERPARAMAGNETIC NANOCOMPOSITES FROM VAPOR PHASE CONDENSATION IN A FLAME

M.R. Zachariah[(1)], M.I. Aquino[(1)], R.D. Shull[(2)] and E.B. Steel[(1)]

[(1)]Chemical Science and Technology Laboratory
[(2)]Materials Science and Technology Laboratory
National Institute of Standards and Technology, Gaithersburg, MD 20899

(Accepted April 1995)

Abstract—*Recent work on the magnetic characteristics of nanometer scale materials has suggested that magnetically isolated nanometer magnetic particles would show magnetic behavior different than those found in the bulk. Such behavior could be explored if such materials could be synthesized in sufficient quantities where the magnetic particles could be isolated from each other via encapsulation within a non-magnetic host. We have investigated application of flame technology for the synthesis of this class of materials. A premixed methane/oxygen flame diluted with nitrogen has been used as the reacting environment in which iron pentacarbonyl and hexamethyldisiloxane were added as the magnetic and non-magnetic precursor materials. The results, based on x-ray diffraction, electron microscopy, Mössbauer effect, and magnetization data have shown that: (i) nanometer composite particles are formed containing 5-10 nm Fe_2O_3, encased in a silica particle whose diameter ranged from 30-100 nm, depending on loading and flame temperature, and (ii) the iron oxide clusters are magnetically isolated and in some cases show superparamagnetic behavior.*

INTRODUCTION

Recent theoretical investigations into magnetic refrigeration technology have suggested a novel approach to obtaining a higher operating temperature than that achievable through conventional paramagnetic materials (1,2). The principles of magnetic refrigeration invoke a magnetic entropy cycle in which application of a magnetic field results in alignment of magnetic moments and a resulting decrease in the magnetic entropy. This implies that the temperature increase (also known as the magnetocaloric effect) thereby rejects heat to the surroundings. Upon removal of the field, the system will absorb heat and complete the refrigeration cycle. One of the primary limitations on the application of such refrigeration cycles at high temperatures is the rapid decrease in the magnetization of traditional bulk materials with increasing temperature, which effectively limits the operating range of such cycles. Shull and coworkers (1,2) have suggested that the magnetic properties of nanocomposites, in which a fine dispersion of magnetic clusters are dispersed in a non-magnetic matrix, has the potential to address this limitation. The basic concept is to combine the properties of ferromagnets, which have a larger magnetization at moderate temperatures than paramagnets, and the much larger magnetocaloric effect of paramagnets. By

using ferromagnetic clusters as individual magnetic domains in which the magnetic spins are aligned, but whose magnetic interaction with a neighboring cluster is weak so that each cluster is magnetically independent, one obtains a *"superparamagnetic nanocomposite"* with a much larger magnetocaloric effect, *i.e.* $dT_{nano} > dT_{para}$.

One of the issues in the practical application of this class of materials is the ability to synthesize sufficient quantities with appropriate and controllable properties. Indeed, this is a problem generic to the whole class of nanostructured materials. In trying to address the specific question posed here, as well as the generic one, we have chosen to focus on the production of an iron oxide-based system based on prior work at NIST. Previous investigations at NIST have focused on the use of liquid-based chemistries that have demonstrated the potential for preparation for this class of materials (3).

In this paper we apply a vapor phase combustion process that has the potential to produce very fine particles in large quantities (4-6). Flame processes have several advantages over both thermal reactors and liquid based chemistries. As a general rule, vapor grown materials possess the highest purity relative to liquid or solid state process. In addition, gas phase flames are the simplest method for producing very high temperatures (< 3000 K), and the methods for scale-up are relatively well understood.

EXPERIMENTAL

The reactor configuration chosen for this work was a premixed methane/oxygen flame as the reaction environment to which iron and silicon bearing precursors were added to obtain a nanocomposite of the magnetic and non-magnetic host, respectively. This configuration was chosen to allow us to very rapidly reach a high temperature in which we would make two immiscible liquids (temperature > 2000 K, based on equilibrium phase diagram (7)) of iron oxide and silicon oxide, which could be very rapidly quenched to preserve this structure and minimize any reaction between the iron and silicon leading to Fe_2SiO_4 ($T < 1500$ K). In addition, this configuration is highly amenable to subsequent *in-situ* characterization and modeling of the gas and particle phases (the subject of a future paper). Figure 1 shows schematically the flame reactor and the particle quenching/collection cooling rod. The precursor species used are liquids at room temperature and were delivered to the reactor as saturated vapors in argon. Iron pentacarbonyl and hexamethyldisiloxane were added as the magnetic and non-magnetic precursor materials. A table of operating conditions is shown below.

TABLE 1
Operating Conditions (in mole fraction units)

Reactants	Flame 1	Flame 2	Flame 3
CH_4	0.08	0.11	0.10
O_2	0.44	0.29	0.33
N_2	0.49	0.60	0.57
T_{adb}	1860 K	2350 K	2450 K

Mole fraction of silicon and iron precursor varied:
$SiO_2(CH_3)_6 < 0.0022$
$Fe(CO)_5 < 0.00055$

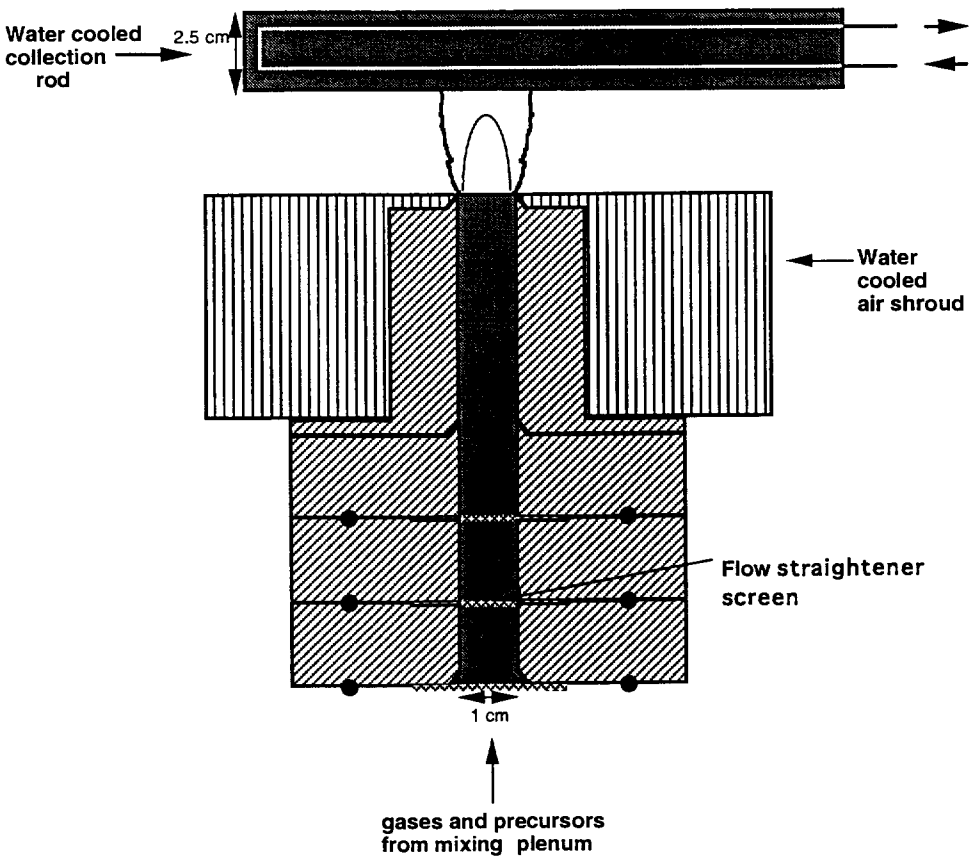

Figure 1. Schematic of flame reactor.

All synthesis conditions were conducted under oxygen-rich conditions at relatively high temperatures to minimize any unwanted carbon contamination in the resulting particles. Particles were collected thermophoretically on a water cooled copper rod that was placed horizontally above the flame, such that the residence time of the flow was less than 5 ms. With the typical flow rates used, particle production rates of up to 2 g/hr were routinely achieved. Flame temperature was measured using a two-color optical pyrometer. Particle samples for transmission electron microscopy were obtained by rapidly injecting a TEM grid directly into the flame at specified heights above the exit nozzle of the reactor. Other *in-situ* characterization, not shown in this paper, include laser induced fluorescence of FeO and SiO gas phase species and laser light scattering from the particles (8,9). *Ex-situ* characterization included Mössbauer, X-ray diffraction (XRD), magnetization, electron energy loss spectroscopy (EELS) and energy dispersive X-ray spectroscopy (EDS).

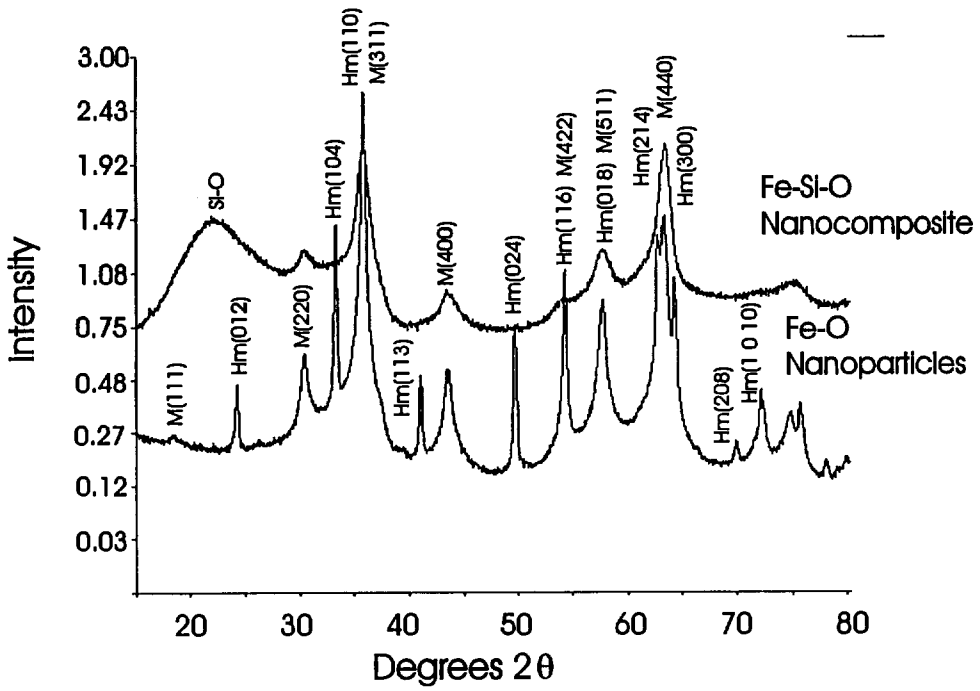

Figure 2. X-ray diffraction patterns of synthesized iron-oxide and nanocomposite. M(hkl) = maghemite/magnetite; Hm(hkl) = hematite.

RESULTS

The basic strategy behind the choice of flame conditions was to run under excess oxygen and high temperature so that we would provide the best opportunity to form γ- Fe_2O_3 (thermodynamically favored at high temperatures), which has the highest magnetic moment of the iron oxides, and prevent the formation of any Fe-Si species. In addition, it is desirable to encapsulate the iron oxide within the silica. High temperatures serve to lower the nucleation rate and promote rapid sintering.

a. Morphology and Chemical Composition

X-Ray diffraction on bulk samples of the powders were used to determine the crystal structure of the Fe/Si/O nanocomposite and Fe/O particles. Figure 2 shows XRD patterns for (data) such samples produced in Flame 2. The XRD pattern from the nanocomposite shows a high background and a broad peak at 22°, indicative of amorphous silica. The more defined lines correspond closely, both in location and relative magnitude, to Fe_3O_4/γ-Fe_2O_3, with line widths suggestive of very small crystallites. A definitive determination of the phase as either Fe_3O_4 or γ-Fe_2O_3 is difficult, due to the fact that the peaks are broad and the overlap of magnetite and maghemite are severe. However, Raman spectra did indicate that the material is mainly γ-Fe_2O_3. By contrast, XRD results, when only the iron precursor are added, indicate the iron particles are

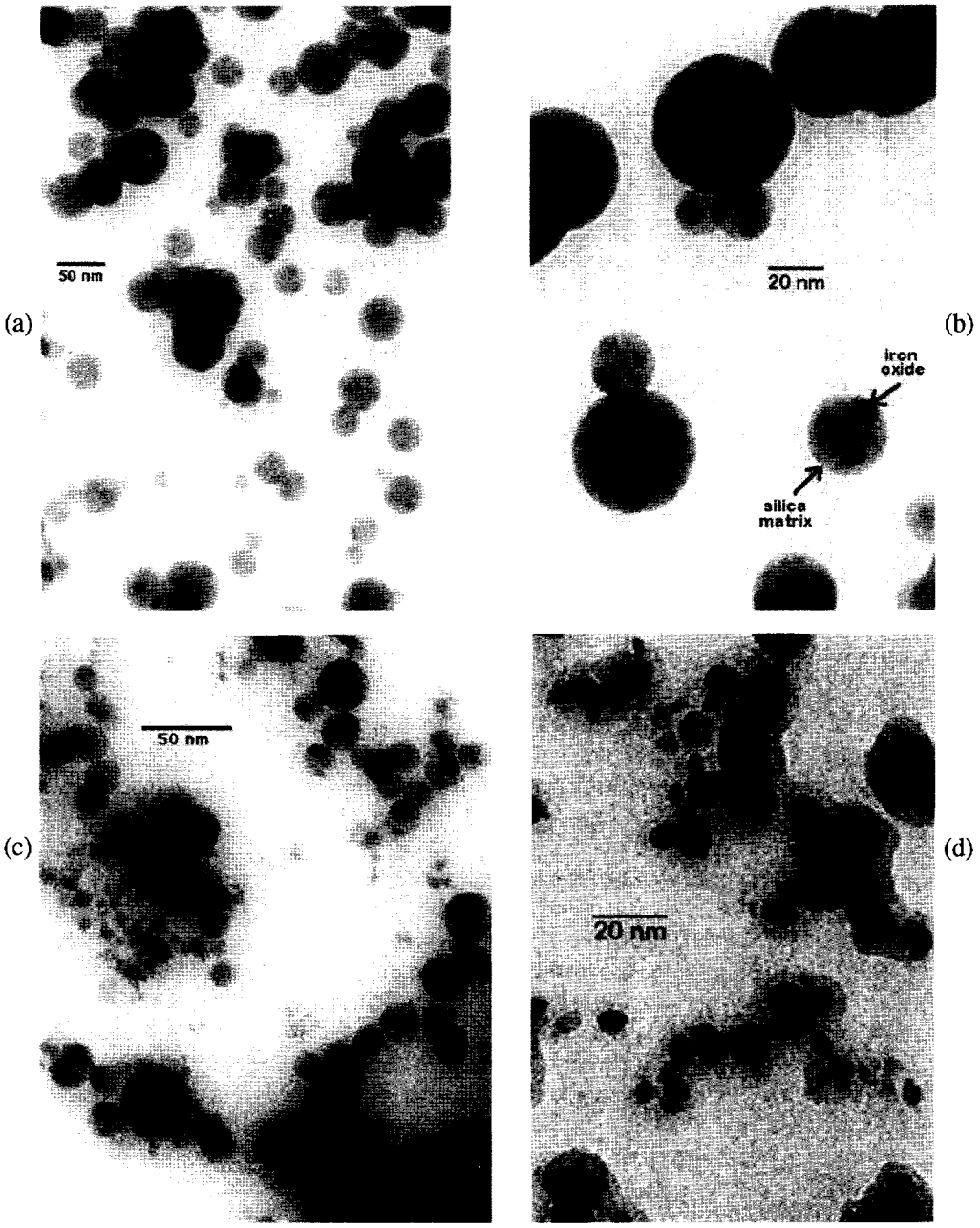

Figure 3. TEM's of iron oxide/silica nanocomposites: (a) iron oxide/silica nanocomposites formed in flame 2 collected at 3.6 cm above reactor nozzle; (b) higher magnification image under same flame conditions as 3a; (c) iron oxide/silica nanocomposites formed in flame 2 collected at 1.5 cm above reactor nozzle (2 mm above flame cone); (d) iron oxide particles (no injection of Si-precursor).

more crystalline than in the nanocomposite. The fact that the XRD patterns of the nanocomposite show a distinct magnetite or maghemite pattern implies that we are making a nonhomogeneous particle in which there are iron rich regions. Interestingly, the chemical state of the iron is essentially equivalent between the nanocomposite and the isolated iron-oxide particle deposits. The clearest difference seems to be that the iron-oxide particles show reflection from at least two phases, hematite and maghemite/magnetite, while the major hematite is not observed in the composite.

A rapid insertion technique (4) allowed us to capture particles directly on the TEM grid at any position in the flame (*i.e.* residence time). Figure 3 shows micrographs of the nanocomposite particles captured at different heights above the exit nozzle of the reactor (total residence time < 5 ms).

The TEM results show that the particles are highly spherical and unagglomerated. The composite particles are composed of two distinct regions. The darker encapsulated regions are iron-rich and are encased with a silicon-rich matrix. The composite particles range in size from 25 - 100 nm in diameter with the inclusions typically less than 10 nm in diameter. Laser light scattering evidence suggests that particles were formed just outside the flame cone, and sampling, despite the poor spatial resolution as compared to the optical means, seems to corroborate these findings. Figure 3c was a sample taken very early in the flow field (at flame cone) and shows the formation of very small clusters, in addition to agglomerates. The wide size distribution results from the fact that the TEM grid, when inserted into the center of the flow field, must traverse the outer boundary of the flame where the flame is cold and the particles have experienced a longer residence time. To minimize this effect, the grid was covered during insertion into the flame and then exposed; however, this method was only marginally successful. The sample shown in Figure 3c was made by this method. An example of particles made under conditions where no silicon precursor is injected is shown in Figure 3d. The most striking feature of the image is the faceted nature of some of the particles and the high degree of agglomeration. In general, there seemed to be two classes of particles. The highly faceted particles tended to be larger and probably experienced a higher temperature, which allowed for faster sintering, and agglomerated particles, which tended to have a much smaller primary particle size down to texture of the carbon support film (< 1 nm) with much lower degree of faceting. The bimodal nature of the distribution is probably attributable to the nature of the sampling (poor spatial resolution). Several of the TEM images in both the composite and single component showed what appeared to be a coating, presumably of a different phase or degree of crystallinity. Future work will be aimed at resolving some of the finer points highlighted here.

By varying the Si/Fe ratio, the separation within each of the magnetic clusters could be varied, while varying the Fe precursor concentration resulted in changes in the average size of the iron containing clusters (inclusions). In many cases, the observed morphology of the composite leads one to believe that the iron particles arrange themselves within the silica matrix in such a way as to maximize the distance between them. EELS analysis did confirm that the dark inclusions within the silica matrix were iron-rich with an Fe/O atom ratio between 0.7-0.9 ($Fe_3O_4 = 0.75$). Evidence of iron inclusion with the silicon matrix went as low as Fe/O = 0.04, indicating that some iron is finely dispersed throughout the matrix, either as very small clusters or in chemically bound form to silicon, although there were regions where no detectable traces of iron were found. However, the fact that the particle sizes and chemical composition of the iron rich regions were similar in both the composite and pure iron particle is suggestive that gas phase chemistry and

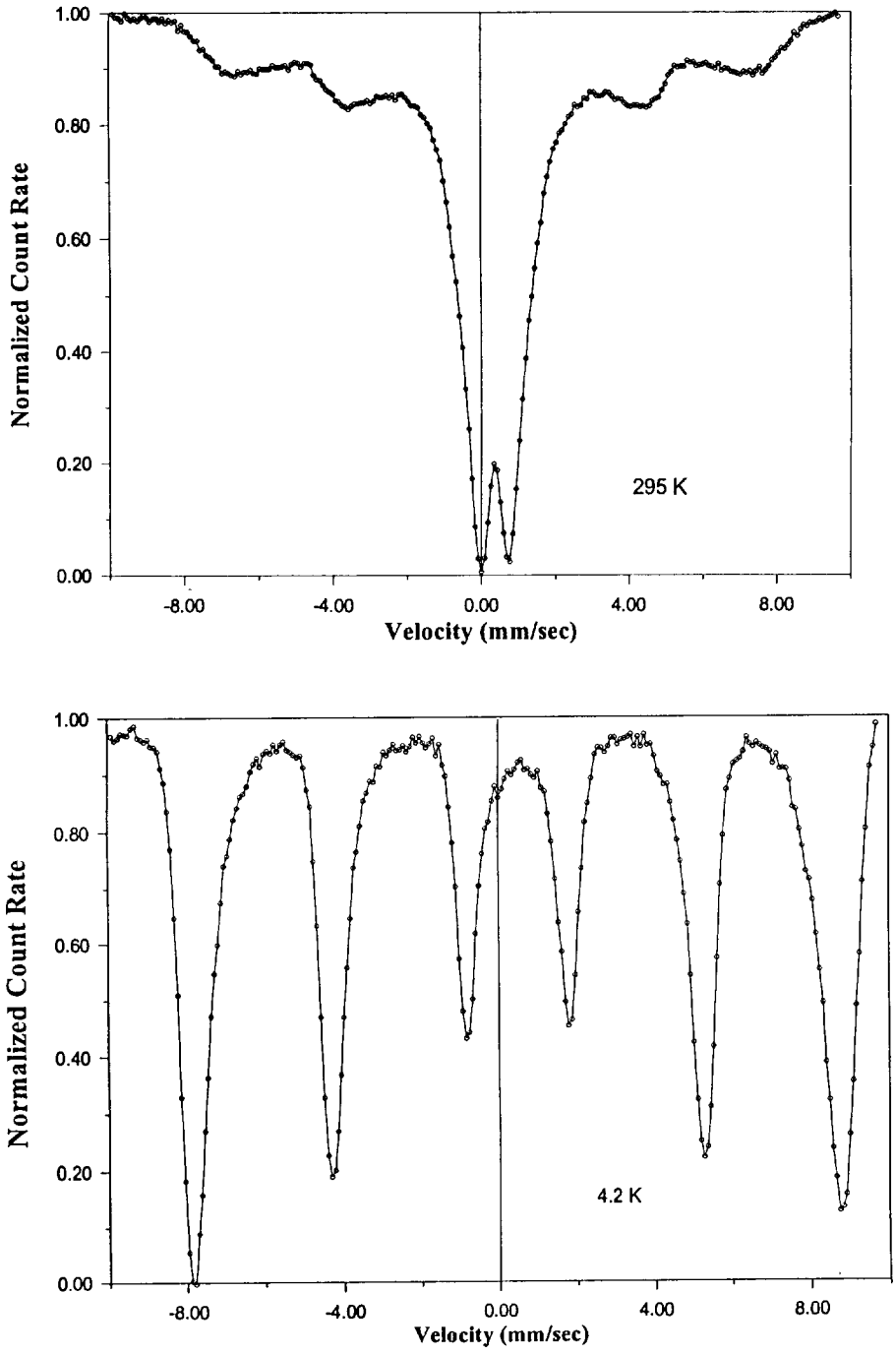

Figure 4. Mössbauer patterns measured with Si/Fe=1.3 at (a) 295 K and (b) 4.2 K.

subsequent homogeneous nucleation is unaffected, even at these high temperatures by the presence of the other nucleation component. This can occur if the nucleation of the iron occurs sufficiently faster than the silicon. Indeed, one of the advantages of the chosen precursors is that the iron precursor decomposes at a lower temperature than the silicon. These results imply that one should be able to vary the extent to which iron inclusions can be incorporated within the matrix without having to change flame conditions.

b. Magnetic Properties

Both magnetic susceptibility and Mössbauer spectra were measured on compacts of these powders. At room temperature, the Mössbauer spectrum for the sample produced in flame 2 with a Si/Fe ratio of 1.3 is shown in Figure 4a. It is a superposition of at least two spectra: (i) a less intense very broad multiple-line spectrum extending to high velocities indicative of varying-sized regions of magnetically-ordered iron oxide, and (ii) a much larger intensity central doublet (possessing an isomer shift of 0.37 mm/sec and quadrupole splitting of 0.74 mm/sec), indicating superparamagnetism similar to that reported by Shull *et al.* (10) for submicron particles of Fe_3O_4. The form of the superparamagnetic particles present in this composite may be deduced from the Mössbauer spectrum measured at temperatures lower than the blocking temperatures of these submicron particles. Upon cooling from room temperature, the magnetic susceptibility data do not indicate the presence of any magnetic phase transition, but the Mössbauer spectrum measured at 4.2 K showed a dramatic change. At 4.2 K, Figure 4b shows that only a single six-line spectrum, although broadened, is observed. The loss of the central Mössbauer doublet on cooling to 4.2 K indicates this temperature is below the blocking temperatures for the submicron iron-oxide particles. In addition, the single spectrum observed at low temperature also implies that the two components, which comprised the room temperature spectrum, are just different size distributions of the same form of iron oxide; the magnetically-ordered portion being simply those large particles with blocking temperatures above room temperature. The measured magnetic hyperfine field of 41.2 MA/m (518 kOe) and 0.51 mm/sec isomer shift are only slightly different from the values (41.7 MA/m and 0.47 mm/sec, respectively) expected for γ-Fe_2O_3. The only other possible identification, consistent with the earlier described x-ray results and the high magnetization possessed by these materials, would have been Fe_3O_4 (magnetite); but then a low temperature Mössbauer spectrum comprised of at least eight readily separated absorption peaks would have been observed. Consequently, the form of the iron oxide embedded in the silica is deduced to be the high temperature form of Fe_2O_3, maghemite.

Magnetization measurements as a function of magnetic field and temperature were performed in a SQUID magnetometer, and the data above 155 K are presented in Figure 5 as a function of the reduced parameter H/T. Separately measured magnetization loops, while the magnetic field was cycled to positive and negative values, showed no hysteresis in this temperature range. The lack of hysteresis and the superposition of all the data in Figure 5 show that this material is indeed superparamagnetic above 155 K with a particle size which is not a function of temperature, consistent with the Mössbauer data described above. Below 155 K, magnetic hysteresis was observed, again consistent with the Mössbauer results. However, it was also found that below this blocking temperature magnetic spin-glass behavior was observed in the magnetization data. This unusual magnetic behavior, which occurs in materials containing small magnetic particles (or clusters), will be the subject of a future paper and therein will be together with this magnetic data, in these magnetic nanocomposites will be presented the subject of a future paper.

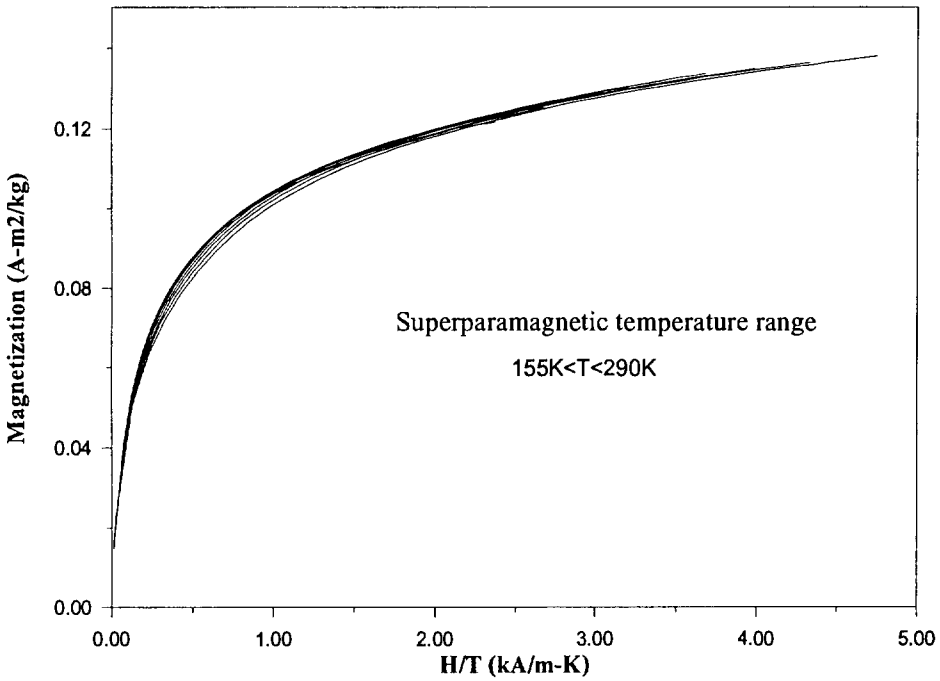

Figure 5. Magnetization (M) vs. temperature normalized magnetic field (H/T) taken between 155 K and 290 K.

CONCLUSION

In this paper we have demonstrated the ability to produce bulk quantities of an iron oxide/ silica nanocomposite possessing superparamagnetic characteristics. The high temperature environment enables one to produce extremely fine particles with high loadings, which are unagglomerated due to the rapid coalescence at these temperatures. For the study considered here, the resulting composite particles contained particles of sizes up to 10 nm of the high temperature phase of iron oxide (magnetite), encapsulated within a nonmagnetic host (silica) particle of less than 100 nm. The particles have shown evidence for superparamagnetism over a wide temperature range.

REFERENCES

1. R.D. Shull, L.J. Swartzendruder and L.H. Bennett, *Proceedings of the Sixth International Cryocoolers Conference,* eds. G. Green and M. Knox, David Taylor Research Center Publ. #DTRC-91/002, Annapolis, Md, p. 231, (1991).
2. R.D. Shull, L.J. Swartzendruder and L.H. Bennett, *Proceedings of the International Workshop on Studies of Magnetic Properties of Fine Particles and their Relevance to Materials Science,* Rome, Italy (1991).
3. R.D. Shull, J.J. Ritter, A.J. Shapiro, L.J. Swartzendruber and L.H. Bennett, J. Appl. Phys. 67, 4490 (1990).

4. M.R. Zachariah, D. Chin, H.G. Semerjian, and J.L. Katz, Comb. Flame 78, 287 (1989).
5. M.R. Zachariah and H.G. Semerjian, AIChE. J. 35, 2003 (1989).
6. M.R. Zachariah and Huzarewicz, J. Mater. Res. 6, 264 (1991).
7. N.L. Bowen and Schairer, Am. J. Sci., 5'th Ser. 24, 200 (1932).
8. M.R. Zachariah and D. Burgess Jr., Aeros. Sci. 25, 487 (1994).
9. B. McMillin, P. Biswas and M.R. Zachariah, *In-Situ Diagnostics of Vapor Phase Growth of Iron Oxide-Silica Nanocomposites: 2-D Planar Laser-Induced Fluorescence and Mie Imaging*, in preparation.
10. R.D. Shull, U. Atzmony, A.J. Shapiro, L.J. Swartzendruber, L.H. Bennett, W.J. Green, and K. Moorjani, J. Appl. Phys. 63 (8), 4261 (1988).